Transporters MCT8 and OATP1C1 maintain murine brain thyroid hormone homeostasis

Steffen Mayerl,[1] Julia Müller,[1] Reinhard Bauer,[2] Sarah Richert,[3] Celia M. Kassmann,[3] Veerle M. Darras,[4] Katrin Buder,[1] Anita Boelen,[5] Theo J. Visser,[6] and Heike Heuer[1,7]

[1]Leibniz Institute for Age Research/Fritz Lipmann Institute, Jena, Germany. [2]Institute of Molecular Cell Biology and Integrated Research and Treatment Center, Center for Sepsis Control and Care (CSCC), Jena University Hospital, Friedrich Schiller University, Jena, Germany. [3]Max-Planck-Institute of Experimental Medicine, Göttingen, Germany. [4]Laboratory of Comparative Endocrinology, Katholieke Universiteit Leuven, Leuven, Belgium. [5]Academica Medical Center, Amsterdam, The Netherlands. [6]Erasmus Medical Center, Rotterdam, The Netherlands. [7]Leibniz Research Institute for Environmental Medicine, Düsseldorf, Germany.

Allan-Herndon-Dudley syndrome (AHDS), a severe form of psychomotor retardation with abnormal thyroid hormone (TH) parameters, is linked to mutations in the TH-specific monocarboxylate transporter MCT8. In mice, deletion of *Mct8* (*Mct8* KO) faithfully replicates AHDS-associated endocrine abnormalities; however, unlike patients, these animals do not exhibit neurological impairments. While transport of the active form of TH (T3) across the blood-brain barrier is strongly diminished in *Mct8* KO animals, prohormone (T4) can still enter the brain, possibly due to the presence of T4-selective organic anion transporting polypeptide (OATP1C1). Here, we characterized mice deficient for both TH transporters, MCT8 and OATP1C1 (*Mct8/Oatp1c1* DKO). *Mct8/Oatp1c1* DKO mice exhibited alterations in peripheral TH homeostasis that were similar to those in *Mct8* KO mice; however, uptake of both T3 and T4 into the brains of *Mct8/Oatp1c1* DKO mice was strongly reduced. Evidence of TH deprivation in the CNS of *Mct8/Oatp1c1* DKO mice included highly decreased brain TH content as well as altered deiodinase activities and TH target gene expression. Consistent with delayed cerebellar development and reduced myelination, *Mct8/Oatp1c1* DKO mice displayed pronounced locomotor abnormalities. Intriguingly, differentiation of GABAergic interneurons in the cerebral cortex was highly compromised. Our findings underscore the importance of TH transporters for proper brain development and provide a basis to study the pathogenic mechanisms underlying AHDS.

Introduction

Monocarboxylate transporter 8 (MCT8) is a specific thyroid hormone (TH) transporter that facilitates the passage of the prohormone 3,3′,5,5′-tetraiodothyronine (T4; also known as thyroxine) and the receptor active form, 3,3′,5-triiodothyronine (T3), across the plasma membrane (1). MCT8 is encoded by *SLC16A2* (hereafter *MCT8*) located on human chromosome Xq13.2. Inactivating mutations and deletions in *MCT8* result in a distinct clinical picture known as Allan-Herndon-Dudley syndrome (AHDS) (2–5).

All affected patients manifest a severe form of psychomotor retardation composed of central hypotonia, spastic tetraplegia, lack of speech development, severe intellectual deficits, and global developmental delays. In addition to the pronounced neurological symptoms, patients exhibit characteristic changes in the serum TH profile, with highly elevated T3 and lowered T4 concentrations. Since 2004, more than 45 families with 125 affected individuals have been reported in the literature, and 1% of cases with the diagnosis of X-linked mental retardation have been estimated to be associated with mutations in *MCT8* (6). However, by which pathogenic mechanisms MCT8 deficiency causes AHDS remains largely unknown.

MCT8 is present in many organs, such as liver, kidneys, pituitary, and thyroid gland, and is also widely expressed in the CNS. Studies in mouse and human brain tissues revealed MCT8 expression in distinct neuronal populations, with the highest mRNA levels in neo- and allocortical structures (e.g., cerebral cortex, hippocampus, and amygdala) as well as in hypothalamic neuroendocrine nuclei (e.g., paraventricular nucleus [PVN]). In addition, MCT8 is found in tanycytes, in choroid plexus structures, and in capillary endothelial cells of the blood-brain barrier (BBB) (7–10). In light of its localization, it has been speculated that MCT8 deficiency compromises the uptake of TH into brain cells, thereby interfering with proper neural migration and differentiation processes during critical stages of brain development.

To get further insight into the pathophysiological role of MCT8, mice with deletion of *Mct8* have been generated and extensively studied (9, 11, 12). These *Mct8* KO animals fully replicated the abnormalities in circulating TH concentrations in AHDS patients and showed a thyrotoxic situation in the liver and kidneys (13). In contrast to AHDS patients, *Mct8* KO mice did not exhibit any overt neurological symptoms. This observation was rather unexpected, as in vivo transport studies have revealed highly diminished T3 uptake into the brains of *Mct8* KO mice (12, 14). However, T4 transport into the CNS was only partially compromised in these animals. Likewise, *Mct8* KO mice displayed only a moderate reduction in brain T3 content, a consequence of a rise in astrocytic type 2 deiodinase (D2) activities, and thus enhanced local T4-to-T3 conversion. It would therefore appear that mice express another T4-specific transporter that maintains almost normal passage of T4 across the BBB and/or the blood-CSF barrier (BCSFB) in the absence of MCT8. The mouse brain would consequently be much less affected by MCT8 deficiency than the human CNS, in which such an alternative route for T4 may not exist.

Which transporter can replace MCT8 in the mouse brain? Organic anion transporting polypeptide 1c1 (OATP1C1; also known as OATP14 or OATP-F), encoded by *Slco1c1* (hereafter *Oatp1c1*), is an intriguing candidate. This transporter accepts preferentially T4 as well as reverse T3 as substrates (15). In mice, OATP1C1 expres-

Conflict of interest: The authors have declared that no conflict of interest exists.
Citation for this article: *J Clin Invest.* 2014;124(5):1987–1999. doi:10.1172/JCI70324.

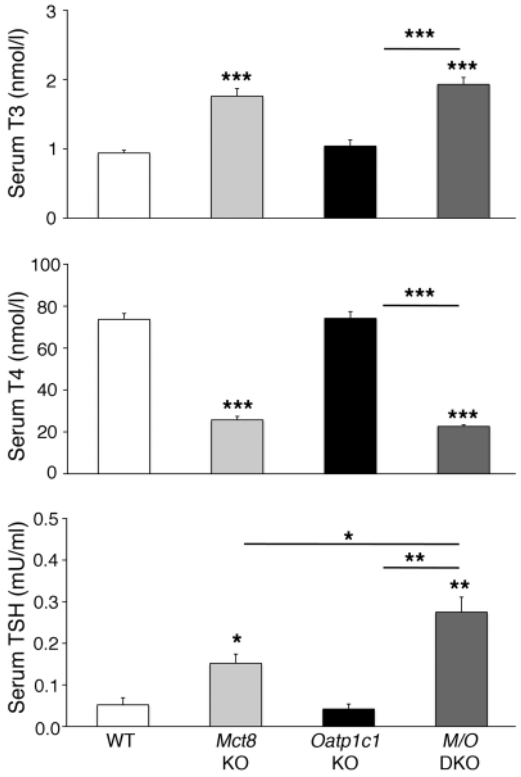

Figure 1
Abnormal serum TH and TSH concentrations in *Mct8*/*Oatp1c1* DKO mice. Serum samples of 8 animals per genotype were analyzed at P21 and revealed increased T3 and decreased T4 serum levels in *Mct8*/*Oatp1c1* DKO mice (*M/O* DKO) as well as in *Mct8* KO mice, whereas *Oatp1c1* KO mice did not exhibit any alterations in serum TH parameters. Serum TSH concentrations were elevated in *Mct8* KO mice and even more so in *Mct8*/*Oatp1c1* DKO animals, which suggests that in the absence of both TH transporters, the HPT abnormalities characteristic of *Mct8* deficiency are even more pronounced. $^{*}P < 0.05$, $^{**}P < 0.01$, $^{***}P < 0.001$ vs. WT, or as otherwise indicated (brackets).

sion is restricted to the CNS, where it is predominantly localized in capillary endothelial cells as well as in choroid plexus structures (16, 17). Most interestingly, OATP1C1 protein could not be detected in BBB endothelial cells isolated from the primate brain (18). This observation is supported by immunohistochemical studies that documented only weak expression of OATP1C1 in capillary endothelial cells in human brain sections (8). Thus, the pronounced expression of OATP1C1 at the BBB and BCSFB of the murine CNS may be the reason for the rather mild brain phenotype of MCT8-deficient mice.

In order to test this hypothesis, we recently generated *Oatp1c1* KO mice (19). These animals develop indistinguishably from WT littermates and do not show any changes in serum TH levels or peripheral TH action. However, the brains of *Oatp1c1* KO mice are characterized by moderately decreased T4 and normal T3 content, which indicates that OATP1C1 contributes markedly to the uptake of T4 into the murine CNS.

Here, we report the generation and analysis of mice with double KO of *Mct8* and *Oatp1c1* (referred to herein as *Mct8/Oatp1c1* DKO mice). In accordance with our hypothesis, these animals exhibited strongly reduced T4 uptake into the CNS that in turn led to a severe form of CNS-specific hypothyroidism and abnormal neuronal differentiation. Based on our findings we propose that the *Mct8/Oatp1c1* DKO mouse represents the most suitable animal model available to date for studying human MCT8 deficiency and testing therapeutic interventions.

Results

Generation of Mct8/Oatp1c1 DKO mice. For the generation of mouse mutants deficient in MCT8 and OATP1C1, *Mct8* KO mice (12) were mated with *Oatp1c1* KO animals (19). Heterozygous offspring of the first generation were intercrossed, producing WT, *Mct8* KO, *Oatp1c1* KO, and *Mct8/Oatp1c1* DKO animals (Supplemental Figure 1A; supplemental material available online with this article; doi:10.1172/JCI70324DS1). WT, single-mutant, and double-mutant mice were born with the expected Mendelian frequency and were indistinguishable from each other during the first 2 weeks of postnatal development. Daily recording of body weight revealed significantly reduced body weight in *Mct8/Oatp1c1* DKO mice starting from P17 (Supplemental Figure 1B). The growth delay persisted after weaning and resulted in a 15%–20% decrease in body weight of adult *Mct8/Oatp1c1* DKO mice compared with WT and single-mutant animals (Supplemental Figure 1C). The growth retardation, however, did not compromise the animals' fertility. Female and male *Mct8/Oatp1c1* DKO mice reproduced normally with a regular litter size.

Analysis of the hypothalamus-pituitary-thyroid (HPT) and somatotropic axes. Determination of serum TH concentrations in P21 animals revealed similarly elevated serum T3 and decreased T4 values in *Mct8* KO and *Mct8/Oatp1c1* DKO mice (Figure 1), which indicated that *Mct8/Oatp1c1* DKO animals show the same abnormalities in the serum thyroid state as do *Mct8* KO mice. Moreover, concentrations of serum thyroid-stimulating hormone (TSH; encoded by *Tshb*) tended to be even more increased in *Mct8/Oatp1c1* DKO mice than in *Mct8* KO mice (Figure 1), although *Tshb* transcript levels were similarly elevated in both mouse models (Figure 2B). These changes may be due to a rise in hypothalamic thyrotropin-releasing hormone (*Trh*) expression, which was previously observed in *Mct8* KO animals (12). In fact, in situ hybridization (ISH) analysis of P21 animals revealed even higher *Trh*-specific signal intensities in *Mct8/Oatp1c1* DKO PVN than in *Mct8* KO PVN (Figure 2, A and B).

In order to study the postnatal differentiation process of the HPT axis in more detail, we examined hypothalamic *Trh* as well as pituitary *Tshb* and *D2* transcript levels at P6, P12, P21, and P33 by ISH. Significantly elevated *Trh* transcript levels were already detected in *Mct8/Oatp1c1* DKO animals at P6 (Figure 2B), which indicated that in the absence of both TH transporters, *Trh*-expressing neurons are already in a pronounced hypothyroid state during early stages of postnatal development. Surprisingly, pituitary *Tshb* expression was significantly reduced in *Mct8/Oatp1c1* DKO mice at P6, but significantly elevated at later time points. Moreover, compared with the single-mutant and WT animals, *D2* expression was slightly elevated in *Mct8/Oatp1c1* DKO mice at P6, whereas at P21, no significant differences between *Mct8* KO and *Mct8/Oatp1c1* DKO mice were noted by ISH or by activity measurements (Supplemental Figure 2A and Supplemental Figure 3A). These results indicated that combined MCT8 and OATP1C1 deficiency leads to deranged development of the HPT axis by early postnatal time points.

Since *Mct8/Oatp1c1* DKO mice were growth retarded, we speculated that the somatotropic axis may also be affected in *Mct8/*

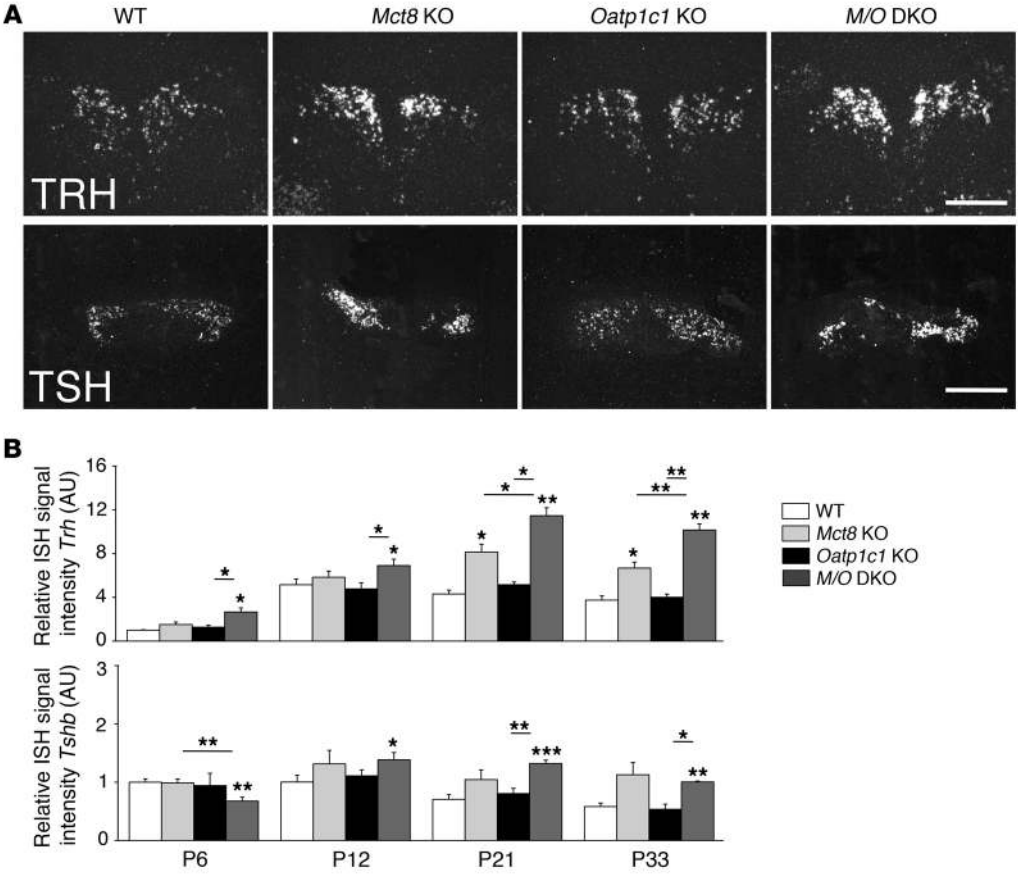

Figure 2
Postnatal development of the hypothalamus-pituitary axis. Brains and pituitaries from male animals (n = 4 per genotype) were collected at different postnatal time points. Hypothalamic *Trh* and pituitary *Tshb* expression were assessed by ISH. (**A**) Darkfield illuminations of brain sections derived from P21 animals illustrated the increase in *Trh* and *Tshb* signal intensities in *Mct8* KO versus *Oatp1c1* KO and WT mice. *Trh* expression was even further upregulated in *Mct8*/*Oatp1c1* DKO animals. Scale bars: 250 μm (*Trh*), 1 mm (*Tshb*). (**B**) This optical impression was confirmed by quantification of relative signal intensities. $^{*}P < 0.05$, $^{**}P < 0.01$, $^{***}P < 0.001$ vs. WT, or as otherwise indicated (brackets).

Oatp1c1 DKO mice. In line with a normal growth curve within the first postnatal weeks, analysis of pituitary growth hormone (*Gh*) mRNA expression by ISH did not reveal any differences at P6 and P12 (Supplemental Figure 2C). However, at P21 (i.e., around the time when *Mct8/Oatp1c1* DKO growth retardation became evident), pituitary *Gh* expression as well as hepatic *Igf1* expression was reduced in *Mct8/Oatp1c1* DKO mice (Supplemental Figure 3A). Moreover, ISH analysis revealed a drop in expression of hypothalamic growth hormone–releasing hormone (*Ghrh*) in *Mct8/Oatp1c1* DKO mice, whereas hypothalamic somatostatin (*Sst*) expression was not altered (Supplemental Figure 3A). Therefore, we hypothesized that in the absence of MCT8 and OATP1C1, the decreased pituitary *Gh* expression is reflective of reduced GHRH stimulation.

TH metabolism and action in liver and kidneys. In order to determine whether *Mct8/Oatp1c1* DKO mice exhibit the same alterations in peripheral TH metabolism as do *Mct8* KO mice, we analyzed the expression of renal and hepatic type 1 deiodinase (*D1*) at P21. Again, *Mct8/Oatp1c1* DKO and *Mct8* KO mice showed similarly elevated *D1* transcript levels in the liver and kidneys, as assessed by ISH and quantitative real-time PCR (qPCR; Supplemental Figure 3, B and C). Since D1 is positively regulated by T3, these increased *D1* mRNA values pointed to a hyperthyroid situation in these tissues. This possibility was further supported by the determination of hepatic expression of another gene whose product is positively regulated by T3, α glycerol-3-phosphate dehydrogenase (*Gpd2*), which also exhibited increased transcript levels in *Mct8* KO and *Mct8/Oatp1c1* DKO mice (Supplemental Figure 3C). Together, these data indicated that in peripheral tissues, *Mct8/Oatp1c1* DKO mice fully replicate the abnormalities in TH metabolism and action that were previously reported in *Mct8* KO animals (11–13).

In vivo T4 transport studies. We previously demonstrated by in vivo transport studies that the uptake of i.p. [^{125}I]T3 into the mouse brain was strongly diminished in the absence of MCT8, whereas the transport of [^{125}I]T4 was only mildly affected (12). Here, we repeated the transport studies by injecting at least 3 adult animals per time point and genotype with 1.2 μCi [^{125}I]T4 i.p. At given time points, the amount of radioactivity in the brain, liver, kidneys, and blood samples was determined by a γ counter and expressed as percentage of the injected dose per gram tissue. No differences among the 4 genotypes were detected in blood and liver samples (Figure 3A), which indicates that neither the absence of MCT8 nor the lack of OATP1C1 affected T4 transport in the blood and into the liver. In the kidneys, *Mct8* KO and *Mct8/Oatp1c1* DKO mice showed a significantly increased accumulation of radioactivity, thereby confirming previous findings in *Mct8* KO animals (13). In both *Mct8* KO and *Oatp1c1* KO mice, accumulation of radioactivity in the CNS was reduced to approximately 50% of WT levels, which suggested that both transporters contribute equally to the passage of T4 into the brain. Most interestingly, uptake of T4 into the brain was strongly reduced in *Mct8/Oatp1c1* DKO mice. Thus, these animals would consequently be expected to display a severe state of hypothyroidism specifically in the CNS.

Analysis of TH content and metabolism in the brain. In order to determine brain TH content, we intracardially perfused P21 animals with PBS, after which forebrains and cerebella were collected and processed as described previously (19). In agreement with

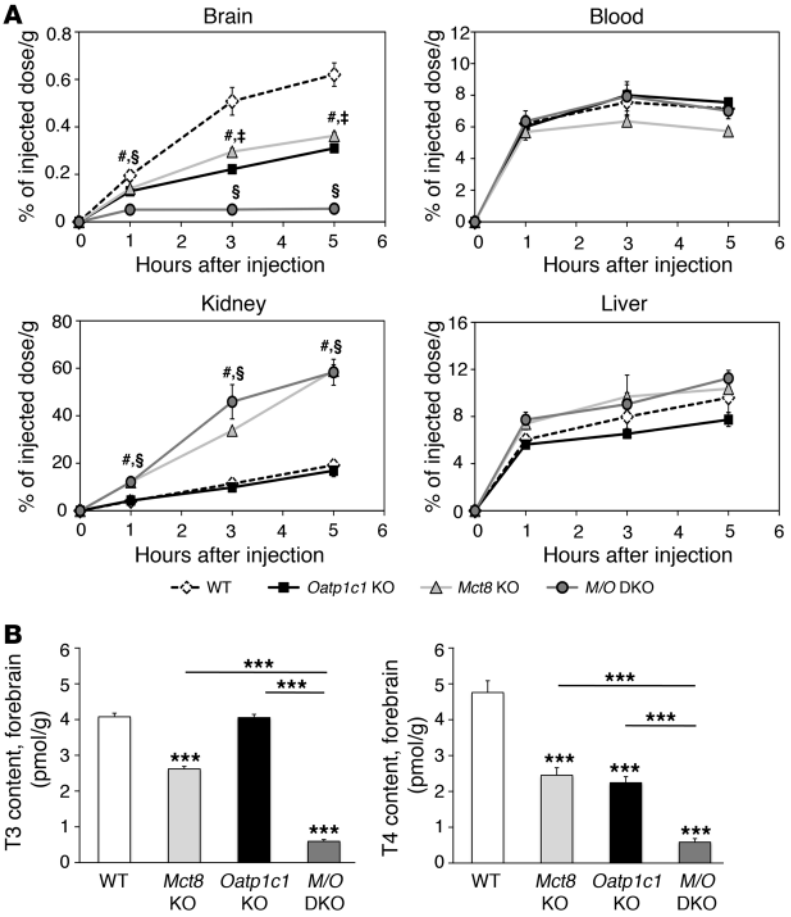

Figure 3

Strongly diminished uptake of T4 into the brain in the absence of MCT8 and OATP1C1. (**A**) For in vivo transport studies, adult animals (n = 3 per genotype and time point) were injected i.p. with 1.2 μCi [^{125}I]T4. A blood sample was obtained, after which animals were perfused with PBS, and brains, livers, and kidneys were collected. The amount of radioactivity was expressed as percentage of the injected dose per gram of tissue. Whereas the amount of radioactivity in blood and liver samples did not differ among mutant groups, *Mct8* KO and *Mct8*/*Oatp1c1* DKO mice showed increased renal radioactivity at all analyzed time points. Most importantly, transport of radiolabeled T4 into the brain was strongly diminished in *Mct8*/*Oatp1c1* DKO mice, whereas in the single-mutant animals, T4 uptake was reduced to approximately 50% of the respective WT levels. $^{\#}P < 0.05$, *Mct8* KO vs. WT; $^{\S}P < 0.05$, *Mct8*/*Oatp1c1* DKO vs. WT; $^{\ddagger}P < 0.05$, *Oatp1c1* KO vs. WT. (**B**) Animals at P21 (n = 8 per genotype) were perfused with PBS before forebrains were collected for determining tissue TH concentrations. The concomitant inactivation of both TH transporters resulted in a pronounced decline of both T3 and T4 to approximately 10% of the levels in WT animals, which indicated that only *Mct8*/*Oatp1c1* DKO mice exhibit a severe hypothyroid state in the CNS. $^{***}P < 0.001$ vs. WT, or as otherwise indicated (brackets).

previous observations, *Mct8* KO and *Oatp1c1* KO mice exhibited an approximately 50% reduction in forebrain T4 levels compared with WT animals, whereas forebrain T3 concentrations were only mildly decreased in *Mct8* KO mice and not altered in *Oatp1c1* KO animals. However, forebrain T4 and T3 values were strongly reduced in *Mct8/Oatp1c1* DKO mice, accounting for only 10% of WT levels (Figure 3B).

The highly reduced TH concentration in *Mct8/Oatp1c1* DKO brains should lead to pronounced alterations in D2 and type 3 deiodinase (D3) activities, as these are negatively and positively regulated, respectively, by TH. Indeed, evaluation of D2 activities in forebrain and cerebellum of P21 animals revealed the highest activities in *Mct8/Oatp1c1* DKO mice, with an almost 10-fold rise compared with WT animals (Figure 4A). Forebrain and cerebellar D3 activities were decreased to a similar extent in *Mct8/Oatp1c1* DKO and *Mct8* KO mice (Figure 4B). We also included brain tissue from athyroid *Pax8* KO mice (which do not produce any TH endogenously; ref. 20) collected at P21, and found that the D2 and D3 activities in forebrain and cerebellum homogenates derived from *Mct8/Oatp1c1* DKO and *Pax8* KO mice were very similar (Figure 4, A and B).

Expression analysis of T3-regulated target genes in the CNS. For monitoring cell-specific changes in T3 concentrations, extensive ISH studies were performed in order to determine the expression levels of well-established T3 target genes. Frontal brain sections of P21 animals were hybridized with radioactively labeled cRNA probes specific for hairless (*Hr*), neurogranin (*RC3*), and aldehyde dehydrogenase 1a1 (*Aldh1a1*), all of which are known to be positively regulated by T3 (21, 22). In addition, we included *D2* in our analysis as a prominent example of a negatively regulated gene. Finally, we examined the transcript levels of mu-crystallin (*Crym*), which encodes an established intracellular TH-binding protein (23, 24). *Hr*-specific ISH signals were slightly reduced in cortical areas of *Mct8* KO animals and strongly decreased in the cerebral cortex of *Mct8/Oatp1c1* DKO mice (Figure 5A). Expression of *RC3*, which is controlled by T3 specifically in the striatum, was strongly downregulated in striatal neurons of *Mct8/Oatp1c1* DKO animals. Likewise, *Aldh1a1*-specific ISH signals were very low in cortical and hippocampal regions of *Mct8/Oatp1c1* DKO mice, whereas endothelial expression of *Aldh1a1* remained unaltered in all mutant animals. In contrast, *D2* ISH signals were visibly elevated throughout the brain only in the absence of both TH transporters. Even expression of *Crym* — which is highly enriched in distinct neurons of the hippocampus, cortex, and striatum — appeared to be increased in *Mct8/Oatp1c1* DKO animals (Figure 5A), which suggested that this TH-binding protein is negatively regulated by T3.

In order to validate these ISH findings, we performed qPCR analysis using whole forebrain samples of P21 animals. In addition to *Mct8* KO, *Oatp1c1* KO, *Mct8/Oatp1c1* DKO, and WT animals, we again included *Pax8* KO mice in our analysis. Inactivation of MCT8 and/or OATP1C1 led to significantly reduced *Hr* and *RC3* transcript levels; the most prominent of these effects were observed in *Mct8/Oatp1c1* DKO mice (Figure 5B), thereby confirming the ISH results. The same, however, did not apply for

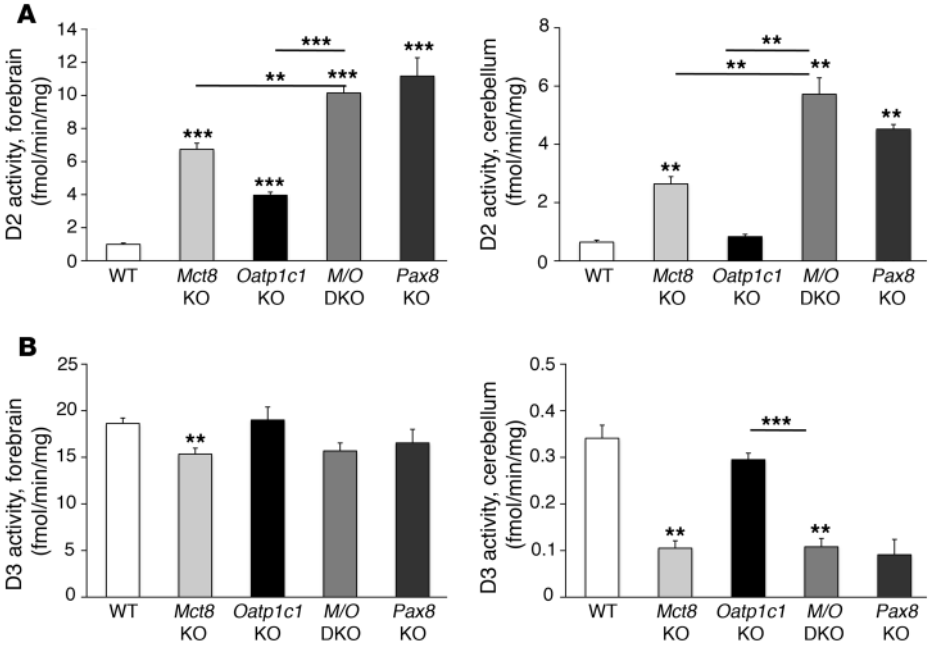

Figure 4
Effect of combined MCT8 and OATP1C1 deficiency on TH metabolism in the CNS. (**A**) Activities of the TH activating enzyme D2, separately measured in forebrain and cerebellar homogenates of animals at P21 (n = 6 per genotype), revealed a more than 10-fold elevation in *Mct8/Oatp1c1* DKO mice, similar to that in athyroid *Pax8* KO mice. (**B**) Determination of D3 enzymatic activities unveiled a similar reduction in *Mct8* KO, *Pax8* KO, and *Mct8/Oatp1c1* DKO animals, whereas D3 activities were not significantly altered in *Oatp1c1* KO animals. $^{**}P < 0.01$, $^{***}P < 0.001$ vs. WT, or as otherwise indicated (brackets).

Crym: qPCR analysis revealed only slightly elevated transcript levels in *Mct8/Oatp1c1* DKO mice, despite a pronounced increase in ISH signal intensities in distinct brain areas. This indicated that *Crym* expression is only altered in selected neuronal populations under hypothyroid conditions. Interestingly, for all genes analyzed in this study, no differences were detected between *Mct8/Oatp1c1* DKO mice and *Pax8* KO animals (Figure 5B), a finding that underscored the severity of the hypothyroidism in the CNS of *Mct8/Oatp1c1* DKO animals.

Delayed cerebellar development in Mct8/Oatp1c1 DKO mice. To study the effect of combined MCT8 and OATP1C1 deficiency on neural development, we histochemically monitored the maturation of different brain areas during postnatal development. Sagittal vibratome sections through the cerebellar vermis were immunostained with an antibody against calbindin D28 (CB), which allows for visualization of Purkinje cells (PCs). PC dendritogenesis, a differentiation process whose dependence on proper TH supply has been well established (25), takes place in rodents within the first 3 postnatal weeks. PCs displayed poor arborization and reduced dendritic growth in sections derived from P12 *Mct8/Oatp1c1* DKO animals, whereas the morphology of PCs derived from *Mct8* KO and *Oatp1c1* KO animals was not altered (Supplemental Figure 4A). However, at P33 and P120, differences in PC morphology were no longer observed in *Mct8/Oatp1c1* DKO mice. Quantification of the thickness of the molecular layer that is primarily determined by the dimension of the PC dendritic tree confirmed the immunohistochemical observations: only at P12 was significantly reduced thickness of the molecular layer noted in *Mct8/Oatp1c1* DKO mice.

Myelination is permanently compromised in Mct8/Oatp1c1 DKO mice. Formation of myelin is another maturation process in the CNS that is compromised under hypothyroid conditions (26). TH has been shown to promote myelination by inducing the expression of proteins such as myelin basic protein (MBP) (27). In order to assess the effect of combined MCT8 and OATP1C1 deficiency on the development of white matter tracts, coronal vibratome forebrain sections were stained with FluoroMyelin, a dye that specifically labels mature myelin sheaths. Signal intensities were visibly lower in the corpus callosum (cc) of *Mct8/Oatp1c1* DKO mice compared with single-mutant and WT animals (Figure 6A). Quantification of the signal intensities in the cc area confirmed the optical impression, revealing significantly reduced values in *Mct8/Oatp1c1* DKO mice at P33 and P120. As a further approach to visualizing myelinogenesis, consecutive brain sections were immunostained with an antibody against MBP. Immunofluorescence signal intensities in the cerebral cortex were quantified, which showed significantly decreased MBP levels in *Mct8/Oatp1c1* DKO mice at all time points. These data indicated that the formation and maturation of myelin sheaths is indeed reduced in the combined absence of MCT8 and OATP1C1.

In order to elucidate the myelination status in closer detail, ultrathin brain sections of P21 WT, *Mct8/Oatp1c1* DKO, and *Pax8* KO mice were processed for transmission EM, and the white matter area comprising the cc at the level of the cingulum bundle was analyzed. WT animals exhibited ubiquitous myelination, whereas *Mct8/Oatp1c1* DKO and *Pax8* KO mice showed a patchy myelination pattern, with many axons remaining unmyelinated (Figure 6B). However, higher magnification revealed a normal ultrastructure of the myelin sheaths of those axons that were myelinated (Figure 6B). The reduced number of myelinated axons may affect the thickness of white matter regions. In order to address this possibility, we performed myelin Gallyas silver impregnation as well as axonal Bielschowsky silver stainings on coronal paraffin sections at P21 and P180 and quantified cc thickness at the level of the cingulum bundle (Figure 6C and Supplemental Figure 4B). At both time points, the width of the cc was significantly reduced in *Mct8/Oatp1c1* DKO mice by both staining methods, which indicated that overall myelin content is permanently reduced in the absence of both TH transporters. Similarly, the size of another major brain white matter tract, the anterior commissure, was reduced in *Mct8/Oatp1c1* DKO animals, albeit to a lesser extent than in the cc (data not shown).

Neuronal differentiation is impaired in the cerebral cortex of Mct8/Oatp1c1 DKO mice. Formation and maintenance of not only the cer-

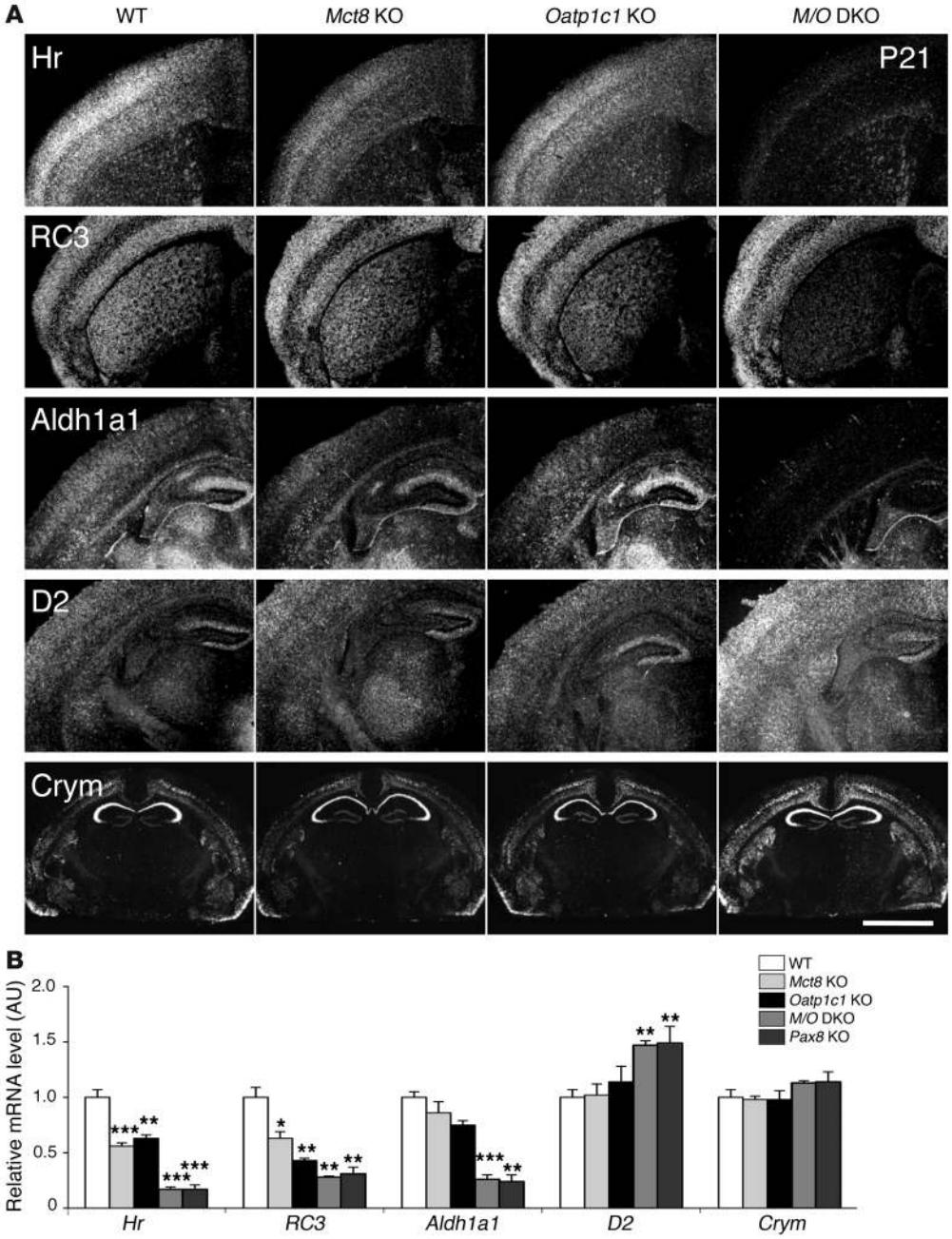

Figure 5
Consequences of combined MCT8 and OATP1C1 deficiency on T3 target gene expression in the CNS. (**A**) ISH studies performed using brain sections at P21 (n = 4 per genotype) revealed for *Mct8*/*Oatp1c1* DKO mice a strong downregulation in the signal intensities for *Hr*, *RC3*, and *Aldh1a1*, all known to be positively regulated by T3. *Hr* expression was most prominently decreased throughout the cerebral cortex, whereas *RC3* expression was highly reduced in neurons of the striatum. In cortical areas, *Aldh1a1*-specific ISH signals were specifically reduced in astrocytes, but relatively unaltered in capillary endothelial cells. Darkfield autoradiograms also illustrated upregulation of *D2* in glial cells. Interestingly, mRNA expression of *Crym*, an intracellular TH binding protein, was elevated specifically in the cortex and striatum. Scale bar: 600 μm (*Hr*, *RC3*, *Aldh1a1*, and *D2*); 3 mm (*Crym*). (**B**) qPCR analysis was performed using forebrain homogenates from P21 animals (n = 4–5 per genotype). Athyroid *Pax8* KO mice were included and showed changes in forebrain gene expression similar to those of *Mct8*/*Oatp1c1* DKO mice. These findings again pointed to a TH-deprived CNS in the absence of MCT8 and OATP1C1. $^*P < 0.05$, $^{**}P < 0.01$, $^{***}P < 0.001$ vs. WT.

ebellar cortex, but also the cerebral cortex, depends on proper TH supply during pre- and postnatal stages. In particular, the differentiation of GABAergic interneurons has been shown to be delayed in hypothyroid rats, as evidenced by reduced parvalbumin (PV) immunoreactivity (28, 29). We therefore wondered whether similar alterations also occur in *Mct8/Oatp1c1* DKO mice and performed immunohistochemical staining for the calcium-binding proteins PV, calretinin (CR), and CB, which serve as distinct markers for specific subgroups of cortical interneurons. In addition, we included antibodies against glutamate decarboxylase 67 (GAD67) in our studies, which allows for visualization of all GABAergic interneurons. NeuN immunoreactivity was used to label all mature neurons. Similar results were obtained in the somatosensory cortex (Figure 7) as well as the motor and the cingulate cortex (data not shown).

Quantification of the immunohistochemical stainings at P33 revealed a significantly reduced number of PV-positive neurons in the somatosensory cortex of *Mct8/Oatp1c1* DKO mice at all analyzed time points (Figure 7A). Moreover, GAD67 immunoreactivity was found to be significantly decreased in *Mct8/Oatp1c1* DKO mice as well (Figure 7B). The reduction in GAD67 immunoreactivity was detected with 2 different antibodies, thereby excluding epitope-specific effects. This observation was surprising, since previous studies in hypothyroid animals as well as in TRα1-mutant animals have not revealed alterations in cortical GAD67 expression (29, 30). In contrast, CB immunoreactivity was decreased in *Mct8/Oatp1c1* DKO mice only at P12; no alterations were ascertained among genotypes at P33 and P120 (Supplemental Figure 5A). A significantly increased abundance of CR-positive neurons

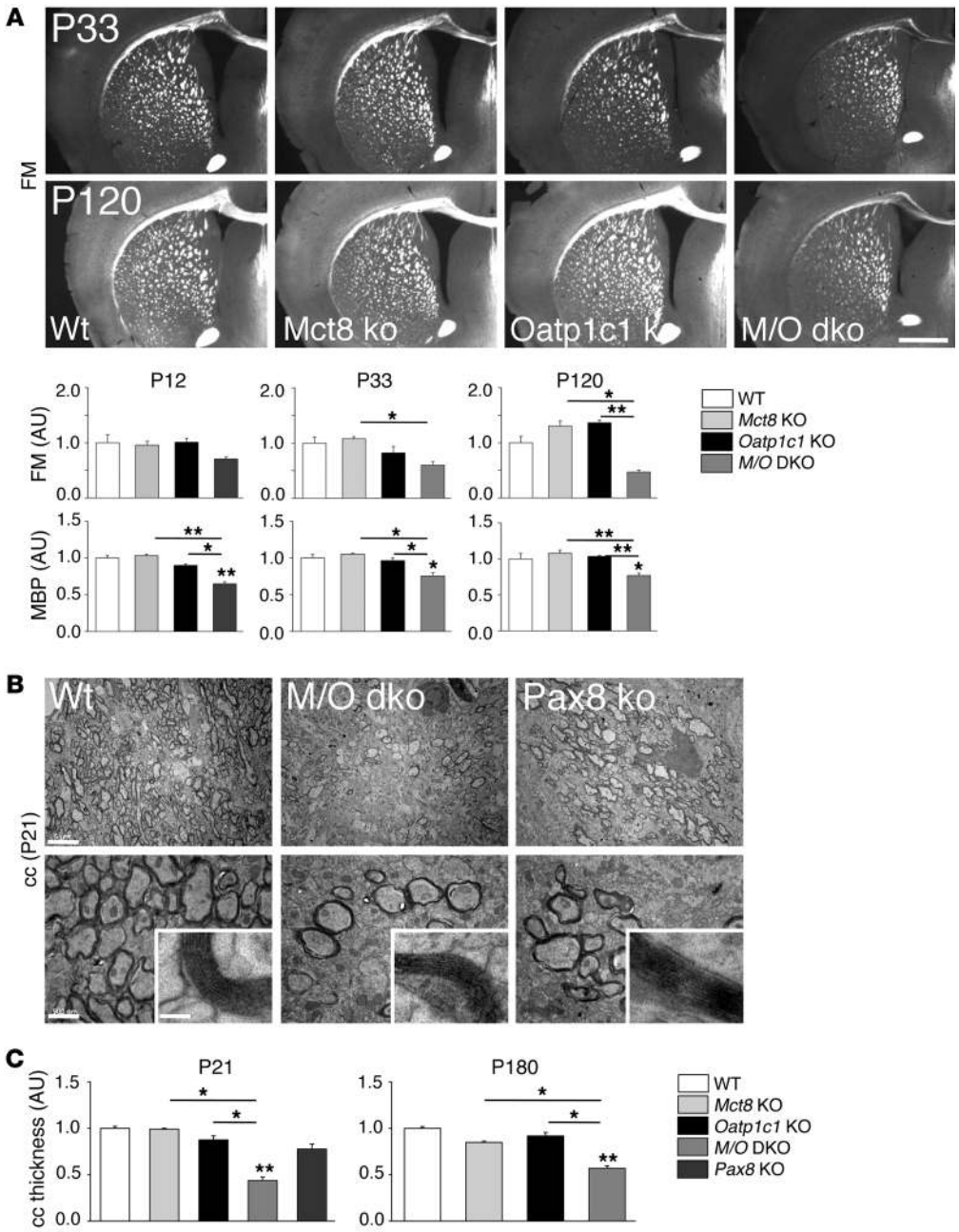

Figure 6

Mct8/Oatp1c1 DKO mice display reduced myelination. (**A**) Frontal vibratome brain sections of male animals (n = 3 per genotype and time point) were stained with FluoroMyelin (FM), a dye that incorporates into myelin sheaths. Additionally, consecutive sections were stained with an antibody against MBP. Quantification of the fluorescence signal densities revealed reduced staining in *Mct8/Oatp1c1* DKO mice at all time points (P12, P33, and P120). Scale bar: 600 μm. (**B**) Ultrathin sections of the medial part of the cc were analyzed by electron microscopy at P21 (n = 3). Compared with WT animals, the number of myelinated axons was visibly decreased in *Mct8/Oatp1c1* DKO mice as well as in athyroid *Pax8* KO mice. However, the ultrastructure of the myelin sheaths appeared rather similar in all genotypes (higher-magnification insets). Scale bars: 5 μm (top); 500 nm (bottom); 50 nm (insets). (**C**) P21 and P180 coronal paraffin brain sections subjected to Gallyas silver staining were used to quantify cc thickness at the cingulum bundle (n = 3). Only *Mct8/Oatp1c1* DKO mice showed decreased cc thickness at either time point. $^*P < 0.05$, $^{**}P < 0.01$, $^{***}P < 0.001$ vs. WT, or as otherwise indicated (brackets).

was observed in *Mct8/Oatp1c1* DKO mice only at P120, although a tendency toward higher numbers was already detectable at P12 and P33 (Figure 7B). NeuN-labeled brain sections were used to quantify the thickness of the different cortical layers (Supplemental Figure 5B). Whereas layers V–VI exhibited similar thicknesses in animals of all genotypes (Supplemental Figure 5A), layers I–IV were significantly thinner in *Mct8/Oatp1c1* DKO animals at all time points (Figure 7B). In summary, our immunohistochemical data pointed to persistent alterations in neuronal differentiation and cortical circuit formation in the absence of MCT8 and OATP1C1.

Mct8/Oatp1c1 DKO mice exhibit pronounced locomotor dysfunctions. As a first approach to assessing the neuromotor performance of TH transporter–mutant mice, we studied the gait of the animals by footprint analysis. Stride length was significantly reduced, and hind paw angle approximately 10° larger, in *Mct8/Oatp1c1* DKO versus WT mice; conversely, *Mct8* KO and *Oatp1c1* KO animals exhibited gait parameters similar to those of WT controls (Figure 8, A and B). These alterations in stride length and hind paw angle were characteristic of cerebellar impairments and have also been found in other hypothyroid animal models (30).

To further examine locomotor behavior, we subjected 4-month-old mice (6–8 per genotype) to an accelerating rotarod test. After an initial training period under constant velocity, animals were tested on 5 consecutive days for their ability to stay on the accelerating rod. With every day of testing, WT, *Mct8* KO, and *Oatp1c1* KO mice learned to stay for a longer time period on the rotating rod. In contrast, *Mct8/Oatp1c1* DKO mice did not improve their motor capabilities during the test period and fell down significantly earlier (Figure 8C).

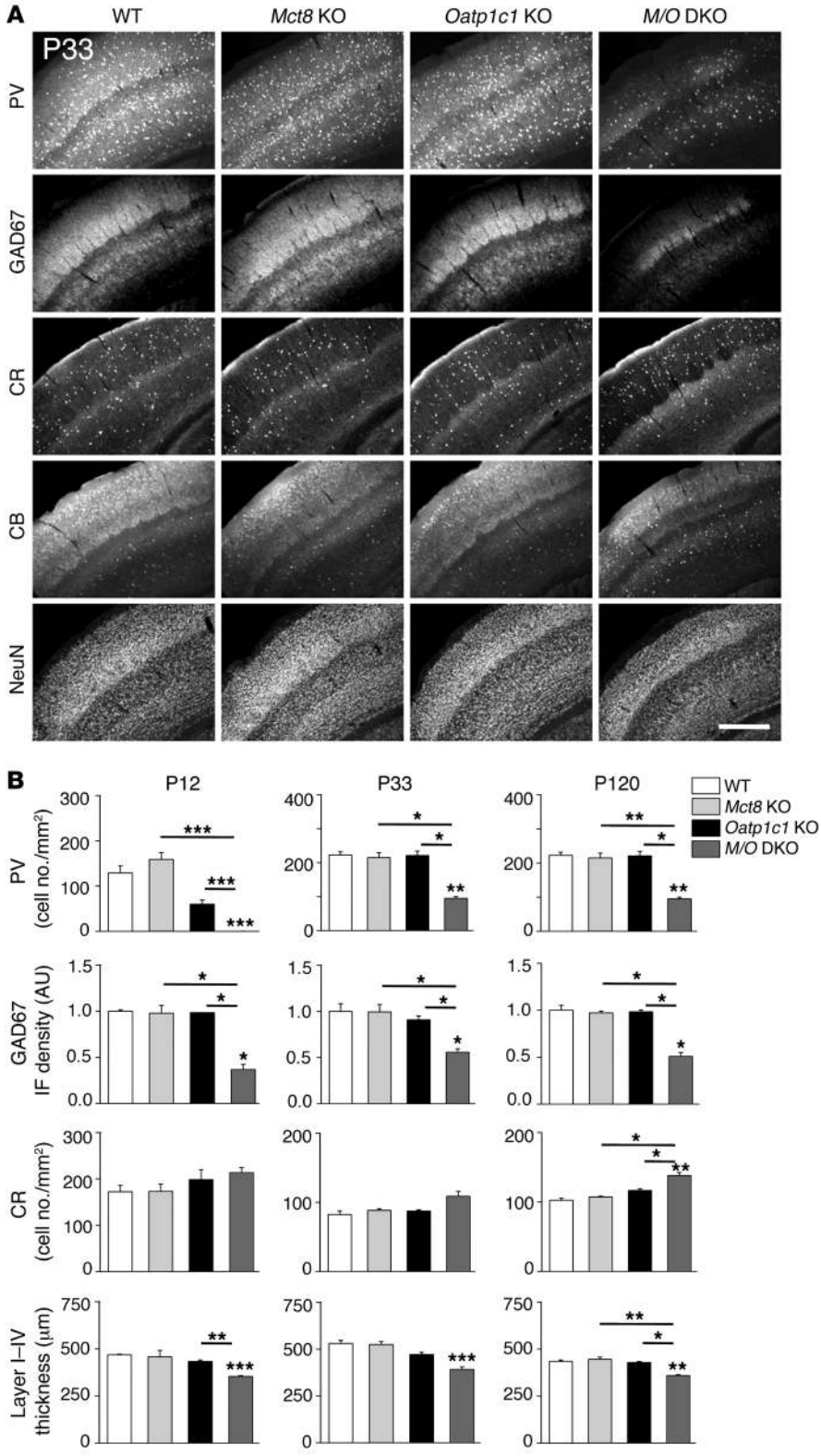

Figure 7
Histological analysis of GABAergic neurons in the somatosensory cortex. Coronal forebrain vibratome sections from perfusion-fixed male mice ($n = 3$ per genotype and time point) were immunostained with antibodies recognizing the calcium-binding proteins PV, CB, and CR; the neuronal transcription factor NeuN; and the GABA-producing enzyme GAD67. (**A**) Representative views demonstrating visibly reduced P33, PV, and GAD67 immunoreactivity in the somatosensory cortex of *Mct8*/*Oatp1c1* DKO mice. Scale bar: 250 μm. (**B**) This optical impression was confirmed by measuring GAD67 integrated fluorescence signal density and counting PV-positive cells using ImageJ. Quantification also revealed a slight increase in the number of CR-positive neurons in *Mct8*/*Oatp1c1* DKO mice. Thickness of the cortical layers was determined in NeuN-stained brain sections and disclosed a thinner layer I–IV in *Mct8*/*Oatp1c1* DKO mice. Overall, these data pointed to pronounced alterations in the cortical GABAergic system in *Mct8*/*Oatp1c1* DKO animals. $^{*}P < 0.05$, $^{**}P < 0.01$, $^{***}P < 0.001$ vs. WT, or as otherwise indicated (brackets).

Since the lower body weight of *Mct8/Oatp1c1* DKO mice may contribute to the poor rotarod performance, we repeated the experiments in order to compare 5-month-old *Mct8/Oatp1c1* DKO and *Mct8* KO littermates with 2-month-old *Mct8* KO mice, whose body weight was similar to that of the *Mct8/Oatp1c1* DKO mice examined. *Mct8* KO animals displayed similar rotarod performance, independent of age and body weight, whereas *Mct8/Oatp1c1* DKO mice again fell off the rotating wheel very quickly (Supplemental

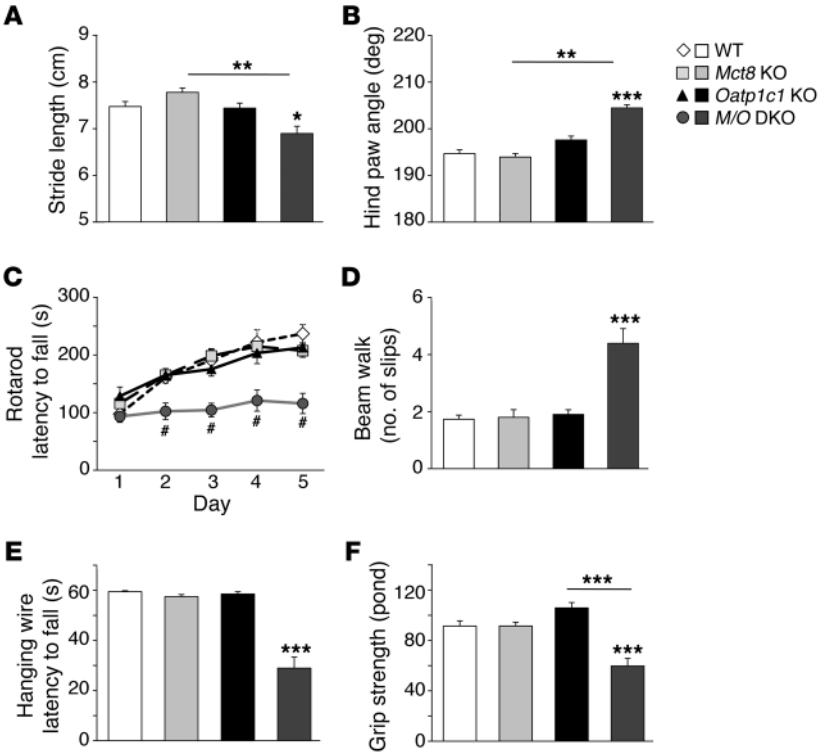

Figure 8
Abnormal gait and severe locomotor deficiencies in *Mct8*/*Oatp1c1* DKO mice. *Mct8*/*Oatp1c1* DKO animals exhibited abnormal gait, as demonstrated by significantly reduced stride length (**A**), and a strongly elevated hind paw angle (**B**) based on footprint analysis. (**C**) Locomotor deficiencies were monitored by a rotarod test using 4-month-old male mice (n = 6–8 per genotype). In contrast to WT, *Mct8* KO, and *Oatp1c1* KO animals, *Mct8*/*Oatp1c1* DKO mice performed poorly on the rod and did not show a learning curve. $^{\#}P < 0.001$ vs. WT. (**D**) In order to assess balance and coordination, mice were monitored while running on a beam 1 cm wide and 100 cm long. Recording the hind limb slips revealed a significantly higher number of errors only in *Mct8*/*Oatp1c1* DKO mice. (**E**) Mice were further subjected to a hanging wire test in order to determine neuromuscular abnormalities. Only *Mct8*/*Oatp1c1* DKO mice were not able to cling on a metal wire for 60 seconds. (**F**) As these findings point to reduced muscle performance, forepaw muscle strength was quantified using a grip strength meter, revealing an approximately 35% reduction in *Mct8*/*Oatp1c1* DKO animals. $^{*}P < 0.05$, $^{**}P < 0.01$, $^{***}P < 0.001$ vs. WT, or as otherwise indicated (brackets).

Figure 6A). This finding rebutted the possibility of a major effect of reduced body weight on locomotor phenotype.

As another approach to monitoring locomotor disabilities and coordination impairments, animals were subjected to a beam walk test: 5-month-old mice (6–8 per genotype) were trained to cross a 100-cm-long square beam 1 cm in width. The number of hind limb slips during the run was recorded, *Mct8/Oatp1c1* DKO mice displayed twice as many slips as the other groups (Figure 8D). Moreover, *Mct8/Oatp1c1* DKO mice also needed significantly more time to cross the beam (Supplemental Figure 6B). Overall, the results of both tests pointed to deficits in fine motor coordination and reduced locomotor activities in *Mct8/Oatp1c1* DKO animals.

Next, a hanging wire test was performed in order to detect alterations in grip strength. Animals were put on a metal wire that was turned upside-down for a maximum of 60 seconds (Figure 8E). WT and single-mutant mice managed to stay on the wire for the entire test period without any obvious problems; instead, they moved around and even groomed themselves. In contrast, *Mct8/Oatp1c1* DKO mice appeared immobile and rarely managed to stay on the wire longer than approximately 30 seconds, indicative of reduced grip strength. To substantiate the latter finding, we quantified grip strength using a high-precision force sensor (Figure 8F). This test also revealed an approximately 35% reduction in forelimb grip strength in *Mct8/Oatp1c1* DKO versus WT mice. These findings suggested that animals with combined MCT8 and OATP1C1 deficiency have pronounced neuromuscular disabilities.

Discussion

Because inactivating mutations in the TH transporter *MCT8* have been linked to AHDS, intensive research activities have been undertaken to clarify why MCT8 deficiency causes severe neurological symptoms and neuromuscular abnormalities in affected patients. These efforts were severely hampered by the fact that information regarding molecular and cellular abnormalities in the CNS of affected patients are still scarce, and that a suitable animal model replicating the phenotype of human MCT8 deficiency was not available. Although mice deficient in MCT8 revealed important aspects regarding the role of MCT8 in peripheral tissues, such as liver, kidneys, and thyroid gland (11–13, 31–33), *Mct8* KO mice did not show any overt neurological symptoms, calling this mouse model into question as an adequate model system for AHDS.

Here, we described the generation and first analysis of mouse mutants that lack the T4-specific transporter OATP1C1 in addition to MCT8. These *Mct8/Oatp1c1* DKO mice fully replicated the abnormal serum TH profile (low T4, high T3, and elevated TSH) characteristic of MCT8 deficiency (Figure 1) and showed a state of hepatic and renal thyrotoxicosis similar to that of *Mct8* KO animals (Supplemental Figure 2). However, in contrast to *Mct8* KO mice, brain development and function was markedly impaired in the absence of both MCT8 and OATP1C1.

Previous studies in mice already revealed the unique function of MCT8 in mediating the passage of T3 into the CNS, whereas T4 transport was found to be mildly affected in the absence of MCT8 (12, 14). At first glance, this finding was rather surprising, since in in vitro assays, MCT8 has been shown to transport T3 and T4 equally well (1). This discrepancy led to the hypothesis that mice express another T4-specific transporter at the BBB and/or BCSFB that ensures delivery of T4 to the CNS, even in the absence of MCT8. That this T4-specific transporter is indeed OATP1C1 was demonstrated unequivocally by our current in vivo uptake studies. Only *Mct8/Oatp1c1* DKO mice exhibited highly diminished passage of peripherally injected T4 into the brain, whereas T4 transport in *Mct8* KO and *Oatp1c1* KO mice was reduced to only about 50% of the WT value (Figure 3). Thus, at

least in the mouse CNS, MCT8 and OATP1C1 mediate the access of TH to the brain.

Although brain TH content was drastically reduced, 10% of WT T3 and T4 levels were still detected in brain homogenates of *Mct8/Oatp1c1* DKO mice (Figure 4). Since animals were perfused with PBS before tissue collection, it is not likely that the TH concentrations found in these brain homogenates only reflect blood contaminations. As one possible explanation, combined MCT8 and OATP1C1 deficiency may not primarily affect the import of TH into capillary endothelial cells, but rather compromise the efflux of TH from endothelial cells into the brain parenchyme and/or astrocytes. Notably, the L-type amino acid transporter LAT1 (encoded by *Slc7a5*) is highly expressed in endothelial cells of the BBB, where it localizes to the luminal site (34). Since LAT1 efficiently transports not only large neutral amino acids, but also TH (35), capillary endothelial cells may still contain significant amounts of TH, even in the absence of MCT8 and OATP1C1. Future studies combining LAT1-mutant mice with animals lacking both MCT8 and OATP1C1 should provide further information in this regard.

We demonstrated by several experimental approaches that astrocytes and neurons of *Mct8/Oatp1c1* DKO mice were clearly deficient in TH. Expression of the astrocytic enzyme D2, which is negatively regulated by T3 at the transcriptional level and even more so by T4 at the posttranslational level, was highly increased in the brains of *Mct8/Oatp1c1* DKO animals, indicative of a pronounced hypothyroid state of astrocytes. Moreover, the transcript levels of several genes known to be positively regulated by TH in distinct subsets of neurons were strongly reduced, to an extent similar to those in athyroid *Pax8* KO animals (Figure 5B). ISH studies also revealed that the hypothalamic transcript levels of *Trh*, which were already elevated in *Mct8* KO animals, were even further increased in *Mct8/Oatp1c1* DKO mice (Figure 2), which indicated that the negative feedback loop of the HPT axis is strongly compromised. Based on this observation, it is reasonable to assume that *Mct8/Oatp1c1* DKO animals exhibit a central resistance to TH, similar to patients with *MCT8* mutations (36).

Congenital hypothyroidism in rodents is linked to various morphological alterations in neuronal maturation, of which retarded cerebellar development is a prominent and well-studied example (37–40). During TH deficiency, the differentiation of basically all cerebellar cell types is delayed. Consequently, the formation of synaptic contacts, which requires a highly synchronized pattern of dendritic and axonal growth, is persistently diminished. A striking hallmark of a congenitally hypothyroid cerebellum is a poorly developed PC with stunted dendrites, a feature that was also observed in *Mct8/Oatp1c1* DKO animals (Supplemental Figure 4A). As the cerebellum represents an important brain area for fine motor control, cerebellar dysfunction is linked to pronounced locomotor deficits, such as ataxia, poor coordination, and incorrectly timed movement. In agreement with disturbed cerebellar development, *Mct8/Oatp1c1* DKO mice exhibited abnormal gait and poor coordination (Figure 8, A–D). Even reduced grip strength, which was a prominent feature of the *Mct8/Oatp1c1* DKO mice (Figure 8F), may be related to cerebellar dysfunction, although abnormalities in neuromuscular transmission cannot be ruled out.

Impaired myelinogenesis is another hallmark of TH deficiency. TH controls the timing of oligodendrocyte development, as it induces oligodendrocyte precursor cells to initiate differentiation processes (41, 42). Moreover, the expression of several myelin-associated proteins, such as MBP, proteolipid protein, or myelin-associated glycoprotein, are directly regulated by TH (43, 44). Therefore, it is not too surprising that, as a result of low TH levels in the CNS, *Mct8/Oatp1c1* DKO mice exhibited reduced myelination caused by reduced white matter tract size, as illustrated by silver stainings (Figure 6 and Supplemental Figure 4B). Such a myelination deficit is expected to compromise neuronal conductance and may also contribute to the locomotor impairments and neuromuscular deficits observed in *Mct8/Oatp1c1* DKO animals.

In addition to these findings, *Mct8/Oatp1c1* DKO mice exhibited rather surprising abnormalities in the cerebral cortex, where immunohistochemical analysis revealed a pronounced and persistent reduction in GAD67 immunoreactivity (Figure 7, A and B), which indicated that the inhibitory cortical GABAergic system is strongly affected. These changes were not restricted to the somatosensory area, but were also observed in other cortical regions, such as the motor and the retrosplenial cortex. In previous studies, TH insufficiency during brain development has been demonstrated to reduce PV immunoreactivity in the cerebral cortex of rats (28, 29), which suggests that only a subgroup of inhibitory interneurons characterized by PV expression — so-called basket and chandelier cells — is sensitive to TH deprivation. Likewise, mouse mutants expressing a dominant-negative TRα1 protein show only a transient reduction in cortical PV immunoreactivity that normalizes after weaning (30). In contrast, PV expression in adult *Mct8/Oatp1c1* DKO mice remained low compared with the respective controls. Moreover, unlike TRα1-mutant animals, *Mct8/Oatp1c1* DKO mice displayed alterations in GAD67 immunoreactivity. Decreased cortical GAD expression has only been reported once for hypothyroid rats (45), which suggests that the phenotype of our TH transporter–deficient mice is rather unique.

Cortical GABAergic dysfunction has been linked to the pathophysiology of various psychiatric disorders, such as schizophrenia, bipolar disorder, and autism (46, 47). PV-positive, fast-spiking interneurons are critically involved in synchronizing the activity of pyramidal neurons and are therefore considered as a key GABAergic system responsible for the control of cortical output (48). Reduced expression of the calcium-binding protein PV leads to asynchronous release of GABA, thereby affecting cortical network oscillations (49). Decreased expression of GAD67, the main GABA-synthesizing enzyme in the CNS, will not only compromise inhibitory transmission, but also affect the maturation of inhibitory synapses, a process that is initiated after the first postnatal week. It is therefore conceivable that in the absence of both MCT8 and OATP1C1, development of the cortical inhibitory system is impaired, which in turn causes augmented and putatively unsynchronized activity of excitatory cortical neurons. The latter hypothesis, however, needs to be further tested by electrophysiological studies.

It also remains to be investigated to what extent the neural abnormalities observed in *Mct8/Oatp1c1* DKO mice can be fully explained by impaired transport of TH via the BBB and/or BCSFB, or whether the contribution of additional factors must be considered. During prenatal development, both TH transporters are present in neuronal precursor cells of the ventricular zone. In fact, analysis of a mouse line expressing an *Oatp1c1* promoter construct–driven cre recombinase and a Rosa26 reporter construct revealed that the *Oatp1c1* promoter is temporarily active in neuronal precursor cells that later develop into a distinct subset of cortical neurons residing in layer 2/3 (50). It is tempting to assume that these neurons might show enhanced sensitivity to alterations in TH levels and that concomitant genetic inactivation of *Mct8*

and *Oatp1c1* may greatly interfere with their differentiation. Such cell-specific effects of combined MCT8 and OATP1C1 deficiency might eventually explain, at least in part, the CNS-specific differences between *Mct8/Oatp1c1* DKO mice and TRα1-mutant animals and may also answer the question of why *Mct8/Oatp1c1* DKO mice exhibited reduced thickness of the outer cortical layers (Figure 7B). Future studies using conditional MCT8 and OATP1C1–mutant mice crossed with a tamoxifen-inducible cre line driven by the *Oatp1c1* promoter should reveal to what extent the simultaneous inactivation of MCT8 and OATP1C1, either at prenatal or at postnatal stages, impairs brain development.

In summary, the *Mct8/Oatp1c1* DKO mouse represents the first animal model showing pronounced TH deficiency in the CNS despite highly elevated T3 concentrations in the circulation, thereby underscoring the physiological importance of TH transporters in providing the brain with sufficient amounts of TH. Unlike single-mutant *Mct8* KO and *Oatp1c1* KO animals, *Mct8/Oatp1c1* DKO mice displayed CNS-specific deficits, such as myelination deficits and pronounced locomotor impairments, that have also been observed in patients. To what extent the *Mct8/Oatp1c1* DKO mouse fully replicates the clinical picture of human MCT8 deficiency cannot presently be assessed, as a biochemical and histopathological analysis of postmortem brain samples of patients has not been reported yet, and even functional MRI data are scarce. Still, *Mct8/Oatp1c1* DKO mice can be considered as the animal model most closely reflecting human MCT8 deficiency. Consequently, we expect detailed studies of pre- and postnatal brain development in these mice to provide further insights on the molecular mechanisms by which TH influences early events in neuronal differentiation or regulates neuromuscular performance. Moreover, *Mct8/Oatp1c1* DKO mice can serve as a valuable tool for testing the efficacy of putative therapeutic interventions in preventing brain damage, since TH treatment is not a useful option for patients with MCT8 deficiency.

Methods

Animals. *Mct8* KO mice were obtained from Deltagen and have been described previously (12). *Oatp1c1*$^{fl/fl}$ mice were generated at TaconicArtemis and mated with a germline deleter cre mouse line in order to obtain *Oatp1c1* KO mice. The targeting strategy, generation, and analysis of *Oatp1c1* KO animals has been published recently (19). *Mct8*$^{-/(-)}$ *Oatp1c1*$^{+/-}$ breeding pairs (C57BL/6 background) were used to generate *Mct8/Oatp1c1* DKO and *Mct8* KO mice. *Oatp1c1*$^{+/-}$ matings (C57BL/6 background) were set up to obtain *Oatp1c1* KO mice and WT littermates. *Pax8* KO mice (mixed background) were generated by breeding *Pax8*$^{+/-}$ animals (20). All mice were provided with standard laboratory chow and tap water ad libitum and were kept at constant temperature (22°C) and controlled light cycle (12-hour light/12-hour dark).

The body weight of 16 litters (5–8 newborn per litter) was monitored daily for the first 3 postnatal weeks. Female and male mice at P21 were killed by CO_2 in order to collect serum samples for TH and TSH determination. In addition, forebrains, kidneys, and pieces of liver designated for ISH analysis were frozen in isopentane cooled on dry ice. Pituitaries were embedded in OCT medium (Sakura Finetek) before being frozen on dry ice. For timeline ISH studies, male mice at P6 and P12 were killed by decapitation, whereas animals at P21 and P33 were killed by CO_2, and tissues were prepared as described above (n = 4 per genotype and time point). Cryosections of coronal forebrain, liver, and kidney (20 μm) as well as pituitaries (16 μm) were thaw-mounted on superfrost slides (Thermo Scientific). Tissues designated for qPCR analysis and measurement of deiodinase activities were rapidly frozen on dry ice and stored at –80°C. For determination of forebrain TH content, animals (n = 8 per genotype) at P21 were deeply anesthetized with isoflurane and perfused intracardially with PBS. Forebrains were rapidly frozen on dry ice and stored at –80°C. Male mice at P12, P33, and P120 destined for immunohistochemical analysis (n = 3 per genotype and time point) were deeply anesthetized with isoflurane and subjected to intracardial perfusion fixation using a solution of 4% PFA in PBS. Whole brains were removed and postfixed for 24 hours with 4% PFA in PBS. Thereafter, brains were washed 3 times in PBS and stored in PBS containing 0.4% sodium azide at 4°C until further processing. See Supplemental Methods for details on animal genotyping.

ISH histochemistry. cDNA fragments corresponding to nt 1,380–1,941 of mouse *Aldh1a1* (GenBank accession no. NM_013467.3), nt 489–1,005 of mouse *Crym* (NM_016669), nt 40–1,055 of mouse *D1* (NM_007860), nt 131–1,045 of mouse *D2* (NM_010050.2), nt 248–445 of mouse *Gh* (NM_008117.2), nt 125–402 of mouse *Ghrh* (NM_010285.2), nt 902–1,598 of mouse *Hr* (NM_021877.2), nt 137–629 of mouse *Igf1* (NM_010512), nt 498–1,005 of mouse *RC3* (NM_022029.2), nt 42–557 of mouse *Sst* (NM_009215), nt 1,251–1,876 of mouse *Trh* (NM_009426.2), and nt 190–445 of mouse *Tshb* (NM_009432.2) were generated by PCR and subcloned into the pGEM-T Easy Vector (Promega). Radiolabeled riboprobes were generated by in vitro transcription using [^{35}S]UTP as labeled substrate (Hartmann Analytik). ISH was carried out as described previously (51). In brief, frozen sections were air-dried, followed by a 1-hour fixation in a 4% phosphate-buffered PFA solution (pH 7.4), and then permeabilized by incubation in PBS containing 0.4% Triton X-100 for 10 minutes. Acetylation was carried out in 0.1 M triethanolamine (pH 8.0) containing 0.25% (v/v) acetic anhydride. Sections were dehydrated, then covered with hybridization mix containing cRNA probes diluted in hybridization buffer (50% formamide, 10% dextran sulfate, 0.6 M NaCl, 10 mM Tris-HCl pH 7.5, 1× Denhardt's solution, 100 μg/ml sonicated salmon sperm DNA, 1 mM EDTA, and 0.5 mg/ml t-RNA). ^{35}S-labeled riboprobes were diluted in hybridization buffer to a final concentration of 1×10^4 cpm/μl. Prior to application, radioactive riboprobes for *Gh*, *Trh*, and *Tshb* were diluted with unlabeled riboprobes (5 ng/μl in hybridization buffer) at ratios of 1:10, 10:1, and 3:1, respectively. Hybridization was performed overnight at 58°C. Slides were rinsed in 2× standard saline citrate (0.3 M NaCl and 0.03 M sodium citrate, pH 7.0) and subsequently treated with ribonuclease A/T1 at 37°C for 30 minutes. Final washes were carried out in 0.2× standard saline citrate at 65°C for 1 hour. For detection of radioactive ISH signals, sections were dehydrated and then exposed to X-ray films (BioMax MR; Eastman Kodak Co.) for 24 hours. Subsequently, sections were dipped in Kodak NTB nuclear emulsion (Kodak) and stored at 4°C for 8 (*Aldh1a1*, *D2*, and *Hr*), 5 (*Crym* and *Ghrh*), 4 (*D1*), 3 (*Gh*, *Sst*, *Trh*, and *Tshb*), or 2 (*RC3*) days. Autoradiograms were developed and analyzed under darkfield illumination. Experiments carried out using the respective sense probes did not produce any ISH signals.

TH, TSH, D2, and D3 activity. Serum T4 and T3 were determined by RIA in P21 animals (n = 8 per genotype) as reported previously (52). Brain T4 and T3 content was measured after extraction of the tissues, as described in detail by Reyns et al. (53). D2 and D3 activities in cerebella and forebrains, as well as D2 activities in pituitary extracts, were assessed as reported previously (52). Briefly, tissues were homogenized in PED10 buffer, and protein concentration was determined by the Bradford method. For D2 activity analysis, homogenate dilutions were incubated with 2×10^5 cpm [^{125}I]T4 in the presence of unlabeled T3. D3 activities were assessed by incubating homogenate dilutions with 2×10^5 cpm [^{125}I]T3. After 30 minutes at 37 °C, reactions were stopped by adding ice-cold ethanol. After centrifugation, supernatants were mixed with 0.02 M ammonium acetate (pH 4) and subjected to HPLC analysis. Radioactivity was monitored using a

flow scintillation detector (Radiomatic A-500; Packard). TSH serum levels were determined using a double-antibody precipitation RIA as previously described (54, 55). Briefly, 25 μl mouse serum, 25 μl PBS containing 0.1% azide, and 100 μl (final dilution, 1:25,000) rabbit anti-rat TSH serum (anti-rat TSH RIA-6; NIDDK) were incubated for 4 hours at RT. Subsequently, 100 μl [^{125}I]rTSH tracer (approximately 15,000 cpm; MP Biomedicals) was added, and the mixture was incubated overnight at RT to allow equilibration. Next, 500 μl donkey anti-rabbit secondary antibody coated onto magnetizable polymer beads (Amerlex M; GE Healthcare) was added, mixed, and incubated at RT for 15 minutes. Samples were centrifuged for 15 minutes at 756 *g* at RT, and the pellets were counted and calculated using Wizard γ counter and RiaSmart software (Perkin Elmer). Mouse standards were prepared by serial dilution of serum pool with high murine TSH (mTSH) with mTSH-0 serum, as described previously (54), and samples were assayed in duplicate.

In vivo transport studies. Uptake analysis was carried out by injecting 2.5- to 4.5-month-old male animals ($n \geq 3$ per genotype and time point) i.p. with 1.2 μCi [^{125}I]T4 (PerkinElmer) in PBS. For injection as well as perfusion, mice were deeply anesthetized with isoflurane. After collecting heart blood, mice were intracardially perfused with PBS, after which brains, livers, and kidneys were collected. To determine the amount of radioactivity taken up by different tissues, organs and blood samples were weighed, and radioactivity was measured in an automatic γ counter.

qPCR. Total tissue RNA was isolated using the NucleoSpin RNA II Kit (Macherey-Nagel). Synthesis of cDNA was performed using the Transcriptor High Fidelity cDNA Synthesis Kit (Roche). To exclude the presence of genomic DNA, 1 sample without reverse transcriptase was included as well. qPCR was performed using iQ SYBR Green Supermix and Multicolor Real-Time PCR Detection System (Bio-Rad). At least 5 samples per genotype were subjected to analysis. As a housekeeping gene for normalization, cyclophilin D (CycD) was used. See Supplemental Methods for primer sequences.

Immunohistochemistry. Perfusion-fixed 50 μm forebrain (frontal) and cerebellum (sagittal) sections of P12, P33, and P120 male mice were cut on a vibratome (Microm). Sections were blocked and permeabilized with 10% normal goat serum in PBS containing 0.2% Triton X-100. Cerebellar sections were stained with a monoclonal mouse anti-CB antibody (1:1,000; Swant), followed by incubation with an Alexa Fluor 555–labeled goat anti-rabbit secondary antibody (Invitrogen) and analysis with a Zeiss Axio Imager Z1 (Zeiss). Consecutive forebrain sections were stained with the following antibodies (all from Millipore): rabbit anti-CB (1:500), rabbit anti-CR (1:500), mouse anti-GAD67 (1:200), rat anti-MBP (1:200), mouse anti-NeuN (1:500), and mouse anti-PV (1:1,000). In addition, a goat anti-human GAD1 antibody (1:40 R&D Systems) was used after blocking the respective tissue sections with 10% donkey serum diluted in PBS containing 0.2% Triton X-100. Subsequently, sections were incubated with respective Alexa Fluor 488– or Alexa Fluor 555–labeled secondary antibodies (Invitrogen) and with Hoechst33258 (1:10,000; Invitrogen) to label cell nuclei. The BrainStain Imaging Kit (Invitrogen) was used to assess the myelin content in 50 μm coronal forebrain vibratome sections according to the manufacturer's protocol. Briefly, sections were permeabilized for 30 minutes in PBS containing 0.2% Triton X-100, then stained with FluoroMyelin green dye (1:300) and DAPI (1:300) in PBS. See Supplemental Methods for details on staining quantification, processing of brain tissue for EM analysis, and Gallyas and Bielschowsky silver staining.

Gait analysis, rotarod, and beam walk test. See Supplemental Methods.

Statistics. Values represent mean and SEM from at least 3 animals per genotype. For multigroup comparisons, 2-way ANOVA was performed (2 × 2 factorial ANOVA; factor A, WT vs. *Oatp1c1* KO; factor B, WT vs. *Mct8* KO) using Daniels XL Toolbox packet for Microsoft Excel. When P values less than 0.05 were received, pairwise comparison between individual groups was done followed by Bonferroni post-hoc testing using Microsoft Excel. A P value less than 0.05 was considered significant.

Study approval. Animal experiments were approved by the local animal welfare committees (TLLV Thüringen, Bad Langensalza, Germany).

Acknowledgments

This work was supported by grants from the DFG (HE3418/5-1, RTG 1715, and SPP1629 [HE3418/7-1]) as well as the Leibniz Graduate School for Aging and Age-Related Diseases (LGSA). The authors thank Alexander Gloria (Friedrich Schiller University), Sabine Landmann (Fritz Lipmann Institute), Mieke van Beeren (Academica Medical Center), Ramona van Heerebeek (Erasmus Medical Center), and Lut Noterdaeme and Lieve Geenen (Katholieke Universiteit Leuven) for excellent technical assistance as well as Frederike Kramer (Fritz Lipmann Institute) for help with gait analysis.

Received for publication April 22, 2013, and accepted in revised form February 6, 2014.

Address correspondence to: Heike Heuer, Leibniz Institute for Age Research/Fritz Lipmann Institute, Beutenbergstr. 11, D-07745 Jena, Germany. Phone: 49.3641.65.6021; Fax: 49.3641.65.6335; E-mail: hheuer@fli-leibniz.de.

1. Friesema ECH, Ganguly S, Abdalla A, Manning Fox JE, Halestrap AP, Visser TJ. Identification of monocarboxylate transporter 8 as a specific thyroid hormone transporter. *J Biol Chem*. 2003;278(41):40128–40135.
2. Dumitrescu AM, Liao XH, Best TB, Brockmann K, Refetoff S. A novel syndrome combining thyroid and neurological abnormalities is associated with mutations in a monocarboxylate transporter gene. *Am J Hum Genet*. 2004;74(1):168–175.
3. Friesema EC, et al. Association between mutations in a thyroid hormone transporter and severe X-linked psychomotor retardation. *Lancet*. 2004; 364(9443):1435–1437.
4. Schwartz CE, et al. Allan-Herndon-Dudley syndrome and the monocarboxylate transporter 8 (MCT8) gene. *Am J Hum Genet*. 2005;77(1):41–53.
5. Friesema EC, Jansen J, Heuer H, Trajkovic M, Bauer K, Visser TJ. Mechanisms of disease: psychomotor retardation and high T3 levels caused by mutations in monocarboxylate transporter 8. *Nat Clin Pract Endocrinol Metab*. 2006;2(9):512–523.
6. Visser WE, Vrijmoeth P, Visser FE, Arts WF, van Toor H, Visser TJ. Identification, functional analysis, prevalence and treatment of monocarboxylate transporter 8 (MCT8) mutations in a cohort of adult patients with mental retardation. *Clin Endocrinol (Oxf)*. 2013;78(2):310–315.
7. Heuer H, et al. The monocarboxylate transporter 8 linked to human psychomotor retardation is highly expressed in thyroid hormone-sensitive neuron populations. *Endocrinology*. 2005;146(4):1701–1706.
8. Roberts LM, et al. Expression of the thyroid hormone transporters monocarboxylate transporter-8 (SLC16A2) and organic ion transporter-14 (SLCO1C1) at the blood-brain barrier. *Endocrinology*. 2008;149(12):6251–6261.
9. Wirth EK, et al. Neuronal 3′,3,5-triiodothyronine (T3) uptake and behavioral phenotype of mice deficient in Mct8, the neuronal T3 transporter mutated in Allan-Herndon-Dudley syndrome. *J Neurosci*. 2009;29(30):9439–9449.
10. Alkemade A, Friesema EC, Kalsbeek A, Swaab DF, Visser TJ, Fliers E. Expression of thyroid hormone transporters in the human hypothalamus. *J Clin Endocrinol Metab*. 2011;96(6):E967–E971.
11. Dumitrescu AM, Liao XH, Weiss RE, Millen K, Refetoff S. Tissue-specific thyroid hormone deprivation and excess in monocarboxylate transporter (mct) 8-deficient mice. *Endocrinology*. 2006; 147(9):4036–4043.
12. Trajkovic M, et al. Abnormal thyroid hormone metabolism in mice lacking the monocarboxylate transporter 8. *J Clin Invest*. 2007;117(3):627–635.
13. Trajkovic-Arsic M, et al. Consequences of monocarboxylate transporter 8 deficiency for renal transport and metabolism of thyroid hormones in mice. *Endocrinology*. 2010;151(2):802–809.
14. Ceballos A, et al. Importance of monocarboxylate transporter 8 for the blood-brain barrier-dependent availability of 3,5,3′-triiodo-L-thyronine. *Endocrinology*. 2009;150(5):2491–2496.
15. Pizzagalli F, Hagenbuch B, Stieger B, Klenk U, Folkers G, Meier PJ. Identification of a novel human organic anion transporting polypeptide as a high affinity thyroxine transporter. *Mol Endocrinol*. 2002;16(10):2283–2296.
16. Sugiyama D, et al. Functional characterization of rat brain-specific organic anion transporter (Oatp14) at the blood-brain barrier: high affinity transporter for

thyroxine. *J Biol Chem*. 2003;278(44):43489–43495.
17. Tohyama K, Kusuhara H, Sugiyama Y. Involvement of multispecific organic anion transporter, Oatp14 (Slc21a14), in the transport of thyroxine across the blood-brain barrier. *Endocrinology*. 2004; 145(9):4384–4391.
18. Ito K, et al. Quantitative membrane protein expression at the blood-brain barrier of adult and younger cynomolgus monkeys. *J Pharm Sci*. 2011;100(9):3939–3950.
19. Mayerl S, Visser TJ, Darras VM, Horn S, Heuer H. Impact of Oatp1c1 deficiency on thyroid hormone metabolism and action in the mouse brain. *Endocrinology*. 2012;153(3):1528–1537.
20. Mansouri A, Chowdhury K, Gruss P. Follicular cells of the thyroid gland require Pax8 gene function. *Nat Genet*. 1998;19(1):87–90.
21. Potter GB, Zarach JM, Sisk JM, Thompson CC. The thyroid hormone-regulated corepressor hairless asoociates with histone deacetylases in neonatal rat brain. *Mol Endocrinol*. 2002;16(11):2547–2560.
22. Iniguez MA, et al. Cell-specific effects of thyroid hormone on RC3/neurogranin expression in rat brain. *Endocrinology*. 1996;137(3):1032–1041.
23. Suzuki S, Suzuki N, Mori J, Oshima A, Usami S, Hashizume K. micro-Crystallin as an intracellular 3,5,3′-triiodothyronine holder in vivo. *Mol Endocrinol*. 2007;21(4):885–894.
24. Friesema EC, Jansen J, Jachtenberg JW, Visser WE, Kester MH, Visser TJ. Effective cellular uptake and efflux of thyroid hormone by human monocarboxylate transporter 10. *Mol Endocrinol*. 2008; 22(6):1357–1369.
25. Heuer H, Mason CA. Thyroid hormone induces cerebellar Purkinje cell development via the thyroid hormone receptor alpha1. *J Neurosci*. 2003; 23(33):10604–10612.
26. Rodriguez-Pena A. Oligodendrocyte development and thyroid hormone. *J Neurobiol*. 1999;40(4):497–512.
27. Barradas PC, Vieira RS, De Freitas MS. Selective effect of hypothyroidism on expression of myelin markers during development. *J Neurosci Res*. 2001; 66(2):254–261.
28. Berbel P, Marco P, Cerezo JR, DeFelipe J. Distribution of parvalbumin immunoreactivity in the neocortex of hypothyroid adult rats. *Neurosci Lett*. 1996;204(1–2):65–68.
29. Gilbert ME, et al. Thyroid hormone insufficiency during brain development reduces parvalbumin immunoreactivity and inhibitory function in the hippocampus. *Endocrinology*. 2007;148(1):92–102.
30. Wallis K, et al. Locomotor deficiencies and aberrant development of subtype-specific GABAergic interneurons caused by an unliganded thyroid hormone receptor alpha1. *J Neurosci*. 2008;28(8):1904–1915.
31. Trajkovic-Arsic M, et al. Impact of monocarboxylate transporter-8 deficiency on the hypothalamus-pituitary-thyroid axis in mice. *Endocrinology*. 2010;151(10):5053–5062.
32. Di Cosmo C, Liao XH, Dumitrescu AM, Philp NJ, Weiss RE, Refetoff S. Mice deficient in MCT8 reveal a mechanism regulating thyroid hormone secretion. *J Clin Invest*. 2010;120(9):3377–3388.
33. Di Cosmo C, et al. Mct8 deficient mice have increased energy expenditure reduced fat mass that is abrogated by normalization of serum T3 levels. *Endocrinology*. 2013;154(12):4885–4895.
34. Roberts LM, et al. Subcellular localization of transporters along the rat blood-brain barrier and blood-cerebral-spinal fluid barrier by in vivo biotinylation. *Neuroscience*. 2008;155(2):423–438.
35. Friesema EC, et al. Thyroid hormone transport by the heterodimeric human system L amino acid transporter. *Endocrinology*. 2001;142(10):4339–4348.
36. Biebermann H, Ambrugger P, Tarnow P, Von Moers A, Schweizer U, Grueters A. Extended clinical phenotype, endocrine investigations and functional studies of a loss-of-function mutation A150V in the thyroid hormone specific transporter MCT8. *Eur J Endocrinol*. 2005;153(3):359–366.
37. Legrand J. Effects of thyroid hormones on central nervous system development. In: Yanai J, ed. *Neurobehavioral Teratology*. Elsevier Science; Amsterdam, the Netherlands; 1984:331–363.
38. Porterfield SP, Hendrich CE. The role of thyroid hormones in prenatal and neonatal neurological development - current perspectives. *Endocr Rev*. 1993;14(1):94–106.
39. Oppenheimer JH, Schwartz HL. Molecular basis of thyroid hormone-dependent brain development. *Endocr Rev*. 1997;18(4):462–475.
40. Bernal J. Thyroid hormones and brain development. *Vitam Horm*. 2005;71:95–122.
41. Barres BA, Lazar MA, Raff MC. A novel role for thyroid hormone, glucocorticoids and retinoic acid in timing oligodendrocyte development. *Development*. 1994;120(5):1097–1108.
42. Tokumoto YM, Durand B, Raff MC. An analysis of early events when oligodendrocyte precursor cells are triggered to differentiate by thyroid hormone, retinoic acid or PDGF withdrawal. *Dev Biol*. 1999; 213(2):327–339.
43. Tosic M, Torch S, Comte V, Dolivo M, Honegger P, Matthieu JM. Triiodothyronine has diverse and multiple stimulating effects on expression of the major myelin protein genes. *J Neurochem*. 1992; 59(5):1770–1777.
44. Farsetti A, Mitsuhashi T, Desvergne B, Robbins J, Nikodem VM. Molecular basis of thyroid hormone regulation of myelin basic protein gene expression in rodent brain. *J Biol Chem*. 1991;266(34):23226–23232.
45. Virgili M, Saverino O, Vaccari M, Barnabei O, Contestabile A. Temporal, regional and cellular selectivity of neonatal alteration of the thyroid state on neurochemical maturation in the rat. *Exp Brain Res*. 1991;83(3):555–561.
46. Powell SB, Sejnowski TJ, Behrens MM. Behavioral and neurochemical consequences of cortical oxidative stress on parvalbumin-interneuron maturation in rodent models of schizophrenia. *Neuropharmacology*. 2012;62(3):1322–1331.
47. Akbarian S, Huang HS. Molecular and cellular mechanisms of altered GAD1/GAD67 expression in schizophrenia and related disorders. *Brain Res Rev*. 2006;52(2):293–304.
48. Lewis DA, Hashimoto T, Volk DW. Cortical inhibitory neurons and schizophrenia. *Nat Rev Neurosci*. 2005;6(4):312–324.
49. Volman V, Behrens MM, Sejnowski TJ. Downregulation of parvalbumin at cortical GABA synapses reduces network gamma oscillatory activity. *J Neurosci*. 2011;31(49):18137–18148.
50. Lang MF, et al. A transgenic approach to identify thyroxine transporter-expressing structures in brain development. *J Neuroendocrinol*. 2011; 23(12):1194–1203.
51. Heuer H, Schafer MK, O'Donnell D, Walker P, Bauer K. Expression of thyrotropin-releasing hormone receptor 2 (TRH-R2) in the central nervous system of rats. *J Comp Neurol*. 2000;428(2):319–336.
52. Friedrichsen S, et al. Regulation of iodothyronine deiodinases in the Pax8$^{-/-}$ mouse model of congenital hypothyroidism. *Endocrinology*. 2003;144(3):777–784.
53. Reyns GE, Janssens KA, Buyse J, Kuhn ER, Darras VM. Changes in thyroid hormone levels in chicken liver during fasting and refeeding. *Comp Biochem Physiol B Biochem Mol Biol*. 2002;132(1):239–245.
54. Pohlenz J, Maqueem A, Cua K, Weiss RE, Van Sande J, Refetoff S. Improved radioimmunoassay for measurement of mouse thyrotropin in serum: strain differences in thyrotropin concentration and thyrotroph sensitivity to thyroid hormone. *Thyroid*. 1999;9(12):1265–1271.
55. van Zeijl CJ, Surovtseva OV, Wiersinga WM, Boelen A, Fliers E. Transient hypothyroxinemia in juvenile glycoprotein hormone subunit B5 knock-out mice. *Mol Cell Endocrinol*. 2010;321(2):231–238.